An investigation of the effects of PVP stabilizing agent on ZnO nanoparticles morphology, crystalline growth, and optical properties

Roshdi Seoudi (rsmawed@yahoo.com)
Physics Research Institute, NRC
Lulua Al-Salem
Qassim University
Doaa Said
Ain Shams University

Article

Keywords: ZnONPs, TEM, XRD, FTIR, UV-Vis spectroscopy, optical properties

Posted Date: June 22nd, 2022

DOI: https://doi.org/10.21203/rs.3.rs-1750601/v1

Abstract

Polyvinylpyrrolidone (PVP) was successfully used as a capping reagent in an aqueous solution to prepare zinc oxide semiconductor nanoparticles (ZnONPs). Transmission electron microscopy (TEM), X-ray diffraction (XRD), Fourier transform infrared (FTIR), and UV-visible spectroscopy were used to determine the effects of PVP concentrations on the morphology, crystallinity, and spectroscopic properties of (ZnONPs). TEM results showed ZnONPs in various shapes (spherical, cubic, hexagonal) and sizes (40 nm-70 nm). PVP concentrations had a significant effect on crystal sizes, full width at half maximum, and X-ray diffraction results of ZnONPs. As confirmed by FTIR spectroscopy, a chemical group of C=O in PVP is electrostatically bound to ZnONPs. A UV-vis spectroscopy experiment was performed in the range of wavelengths (300 nm - 800nm), an energy gap study was conducted based on Tauc's relation, and an Urbach energy calculation was conducted. In addition to improving morphology and crystalline growth, PVP concentrations contributed to improvements in optical properties, which are beneficial for the practical application of ZnONPs.

1. Introduction

Recent years have seen increased interest in the synthesis, characterization, and study of semiconductor nanostructures due to their unique optical, electrical, and magnetic properties [1]. Nanoparticles of zinc oxide (ZnONPs) can be used as semiconductor nanomaterials with stable chemical and thermal properties. Furthermore, its direct bandgap is wide, and its exciton binding energy is high [2–5]. In addition to their unique properties (ZnONPs), they can be used for many different applications, including ultraviolet emitting diodes, cathode ray phosphors, and transparent conductors for photovoltaic cells, chemical sensing, protective films from harmful radiation, and ultrafast nonlinear optical devices [2]. ZnONPs can be prepared using a variety of methods, including chemical processes such as direct co-precipitation and homogeneous precipitation [6], hydrothermal processing [7], the sol-gel method [8], and thermal decomposition of organic precursors [9]. Polymers were used as a capping agent for nanoparticle composites and extensively studied to improve the optical and electrical properties of the composites. ZnO nanoparticles were obtained with a large surface area and high surface energy. Metal ions can be reacted with polymers by the complex or ion-pair formation and polymers can be designed to interact with specific semiconductor nanoparticle properties. Polymers are thus excellent stabilizers [10]. By adding PVP as a capping molecule, when added to reaction mixtures, polyvinylpyrrolidone (PVP) attaches to the surface of growing particles and prevents the particles from further growing, either by electrostatic or steric repulsion. A surface-regulating polymer such as PVP is believed to play a crucial role in the prevention of flocculation of particles and the control of particle morphology and size [11, 12]. The free energy of the ZnO surface is reduced by adding nitrogen (N) and oxygen (O) to PVP, which easily attaches to the ZnO surface. The crystal growth is slowed down as a result. By adsorbing PVP on specific crystalline surfaces, the growth rate of these particles is significantly reduced, resulting in nanoparticles. For hybrid solar cell applications, poly (3-hexylthiophene) capped ZnO nanoparticles are blended with PVP [13]. Compared with their bulk counterpart, nanoparticles possess a greater surface-to-volume ratio.

The surface chemistry of nanoparticles is crucial since more atoms and molecules are arranged on their surfaces [14]. ZnO nanoparticles (NPs) with oxygen vacancies, especially those with oxygen vacancies, have been studied extensively in the past few years, both in synthesis, growth, and defect engineering [15–17]. A variety of capping agents has been used to modify the surface of ZnO nanoparticles to encapsulate defects and reduce their number [18, 19]. In particular, we attempted surface modification in ZnONPs with polyvinyl pyrrolidone (PVP) [20–23] applied to bulk-heterojunction polymer solar cells (PSCs) as an electron transport layer (ETL); surface modification improved the trap-induced defects due to oxygen defects on the surface, thereby preventing the trapping of electrons and reducing of performance. The chemical precipitation method has been used to synthesize ZnO nanoparticles with different concentrations of polyvinylpyrrolidone (PVP). TEM and XRD analyses were performed on samples of as-prepared ZnO to determine the effects of PVP concentration on particle size and crystal growth. Based on FTIR spectra, it can be explained how ZnONPs interact with PVP. By using UV-Vis spectra, we studied the absorption spectra, the energy gap was determined by Tauc's relationship, and its Urbach energy was calculated.

2. Experimental

2.1 Chemicals

Sodium hydroxide (NaOH), zinc nitrate hexahydrate ($Zn(NO_3).6H_2O$), and polyvinylpyrrolidone (PVP) $(C_6H_9NO)_n$ with a molecular weight of 58,000 g/mol were purchased from Sigma-Aldrich.

2.2. Synthesis of ZnO nanoparticles

Polyvinylpyrrolidone (PVP) was used as a reducing agent and stabilizing agent for the preparation of zinc oxide nanoparticles (S1). A volume of 300 mL of $Zn(NO_3).6H_2O$ (0.1M) was heated continuously to 60 ^oC for 20 minutes under magnetic stirring. The reaction was then stirred with magnetic stirring for 20 minutes along with 5 mL of PVP (0.5%). The pH was then adjusted by adding NaOH (0.2 M) drop by drop until it reached 7. This reaction lasted for 20 minutes before stopping. After precipitation, the resultant solution was filtered and washed three times with distilled water and ethanol before being dried in the air. After drying in the air, the residue was dried in an oven at 100°C for 6 hours. Using a gate mortar, the white was ground for 30 minutes to obtain a fine powder. Samples (S2-S5) were synthesized using the same procedure but at different PVP molar ratios (10, 20, 30, and 40 mL). Figure 1 shows all steps involved in the preparation of ZnO nanoparticles.

2.3. Samples Characterization

The sample morphology and particle size were analyzed by a transmission electron microscope (TEM). For the measurements, 10 mL of the solution was poured onto copper grids coated with carbon and allowed to air dry. Samples were performed using a JEOL JEM-1100 microscope (JEOL Ltd., Tokyo, Japan) equipped with a tungsten thermionic gun operating at a 100-kV accelerating voltage. TEM images were acquired using a CCD camera. The X-ray diffraction pattern was measured using CuKα radiation at

40 kV and 40 mA and λ value of 1.5406 Å. At a speed of 0.02°/s, the samples were scanned over 2θo range from 30° to 90°. Scherrer's formula was used to calculate the crystal size of the nanoparticles. An Infrared Fourier Transform Spectrometer, model 300E, was used to obtain vibrational spectra. A thermal-scientific Evolution 220 spectrophotometer (UV.-VIS-NIR) was used to measure surface plasmon resonance with a resolution of 2 nm.

3. Rustles And Discussion

3.1: TEM and Particle Size Analysis

TEM images of ZnONPs were examined to study their morphology, and shapes, and to estimate their sizes (Fig. 2). The hexagonal, spherical, cubic, and cone shapes of the ZnO nanoparticles can be seen in image (A). The particles in the image (B) are nearly spherical, rod-shaped, and arranged in a star. In the image (C), ZnO nanoparticles may have spherical, cube-like, rod-like, and flower-like shapes, and some shadows can be seen surrounding the particles, possibly indicating the presence of PVP surfactant. The particles in an image (D) appear hexagonal in shape. There are a few other forms seen

in the image (E), including short rods, spheres, fibers, and hexagonal shapes. The average diameter of ZnONPs was measured for a range of PVP concentrations (5, 10, 20, 30, and 40 mL) at diameters of 47, 60, 40, 63, and 70 nm. ZnO nanoparticles increased in size with increasing PVP except at 20 mL, where they decreased.

3.2: Analyzing X-Ray Diffraction

Figure 3 displays the X-ray patterns of ZnONPs which were capped by different concentrations of PVP as a surfactant. The diffraction peaks are visible at $2\theta^{o} =$ 31.69°, 34.35°, 36.17°, 47.41°, 56.40°, 62.55°, 66.11°, 67.68°, 68.78°, 72.29°, and 76.66° which correspond to the plans (100), (002), (101), (102), (110), (103), (200), (112), (201), (004), and (202). These results are consistent with those published in (International Center for Diffraction Data, JCDS 36-1451) [24]. Diffraction peaks at $2\theta°$: 31.690, 34.3, and 36.170 are consistent with the hexagonal Wuritize structure of ZnO nanoparticles [11]. Comparing the diffraction patterns of all concentrations of PVP, the increase in intensity indicates an improvement in crystallinity due to the larger particle sizes, except for the PVP concentration of 20 mL. High purity of ZnONPs results in no impurity peaks. The crystalline size was calculated for each sample using the Debye-Scherrer equation:

$$D = \frac{k\lambda}{\beta cos\theta}$$

1

where k is Scherrer constant (= 0.9), λ is the X-ray wavelength = 1.54056 A° of CuK_{α} A radiation source,β is the peak width of half maximum (FWHM), and$\theta°$ is the Bragg's As a result of multiplying each crystal size by its maximum intensity peak, the average crystalline size is computed by dividing each peak by the

sum of the calculated crystal sizes. The average crystalline size was (22.9, 23.43, 20.55, 24.13, and 27.34 nm) at PVP (5, 10, 20, 30, and 40 mL), respectively. Based on the relationship between the intensity value and crystallinity, it can be concluded that the low crystallinity at 20 mL of PVP is due to low crystalline size. These results are in line with the results from TEM.

3.3: FT-IR Study

To understand PVP as a surfactant and how it binds to the surface of ZnO nanoparticles, FT-IR spectra of PVP and PVP-coated ZnONPs were recorded. The FTIR of ZnONPs prepared for different molar ratios of PVP is shown in Fig. 4. There was a strong transmittance peak at about 3460 cm^{-1} in the PVP, indicating O-H stretching vibration. With increasing PVP concentrations up to 20 mL, the band of PVP-capped ZnONPs was

shifted to a lower wavenumber at 3380 cm^{-1}. As for PVP concentration increases, hydrogen bonds may be formed at the ZnONPs/PVP interface. A C-H stretching vibration in PVP is responsible for the strong and weak bands observed in the range (2931 cm^{-1} – 2800 cm^{-1}). PVP has a band at 1628 cm-1 that corresponds to its carbonyl group. There is a new transmittance peak measured at 1504 cm^{-1} in PVP-capped ZnONPs that may be caused by zinc carboxylate stretching vibrations. C-H, C-C, and C-O bonds exhibit bending in-plane vibration modes in PVP at 1390 cm^{-1}. It was determined that covalent bonds of PVP with ZnO nanoparticles caused this band to shift to 1384 cm^{-1} in ZnONPs/PVP. In this band, the intensity increases with increasing PVP concentrations on ZnO surfaces, suggesting that PVP contributes to the increase of surface hydroxyl groups. C-O stretching vibrations are responsible for the band at 1044 cm-1. A small peak was observed in the range (900–1100 cm-1), which is explained by C-N bending vibrations and CH2 attachment to the pyrrole ring in PVP. There is probably a band at ~ 879 cm-1 that corresponds to the carbonate group, commonly observed in the air or indicated to C-H, C-C, C-N, or C-O out-of-plane bending vibrations of PVP. It is clear that the transmitted band at 439 cm-1 is influential. Several

characteristic stretching vibrations of Zn–O were assigned to this peak [27]. There is a summary of all the transmittance peaks and their assignments for all amounts of PVP (5mL – 40mL) in Table 1. FTIR measurements showed coordination between zinc oxide nanoparticles and PVP stabilizers through nitrogen and oxygen atoms.

Table 1
Wavenumber and assignment groups of ZnONPs prepared at different PVP concentrations

Wavenumber (cm^{-1})						Assignment
PVP	PVP = 5 mL	PVP = 10 mL	PVP = 20 mL	PVP = 30 mL	PVP = 40 mL	
3460	3380	3378	3372	3377	3391	O-H stretching vibration
2931	2931	2931	2931	2931	2931	C-H stretching vibration
1634	1628	1628	1628	1628	1628	C = O stretching vibration
-	1504	1503	1501	1503	1503	zinc carboxylate stretching vibration
1384	1384	1384	1384	1384	1384	C-H, C-C, or C-O bending vibration
1050	1044	1044	1044	1044	1044	C-O stretching vibration
832	832	832	832	832	832	C-N bending vibration
-	439	442	442	451	446	Zn-O stretching vibration

3.4 UV-Vis spectroscopy

UV-vis spectroscopy was performed to investigate ZnO nanoparticles. Pesika et al. demonstrated that bulk zinc oxide exhibits an optical absorption at 388 nm [28]. ZnONPs synthesized with various PVP concentrations are shown in Fig. 5, while Table 2 shows maximum absorption bands with PVP concentrations (5, 10, 20, 30, and 40 mL) at (363.56, 366.64, 362.90, and 374.90 nm). Furthermore, the quantum confinement effect of ZnONPs was demonstrated by Mun Lam et al. [29]. Compared with bulk, it was found that ZnO was synthesized at the nanoscale based on the quantum confinement effect.

Furthermore, the change in band position of ZnONPs indicates that particle size depends on the concentration of PVP. The absorption band shifted from red to blue with increasing PVP concentrations, indicating increased particle sizes except for 20 mL PVP. This band position was blue-shifted at 362.9 nm. In our study, PVP was used as a surfactant to accommodate changes in viscus condition and to reduce ion diffusivity. Therefore, it can alter nanoparticle sizes, morphology, crystallinity, and other surface properties according to their molecular structure [30, 31]. Due to the effects of diffusion and the attachment rates of PVP to the surface of ZnONPs, particle size increased with the raised of PVP (5, 10, 30, and 40 mL). When the amount of PVP is increased, the growth process is accelerated. Consequently, PVP can increase the size and enhance the crystallinity of ZnO nanoparticles. In contrast, the particle size decreased at PVP (20 mL), which can be explained by the high viscosity of PVP, which produces a more significant steric hindrance effect that prevents the tiny particles from growing into larger solids. As a

result, nanoparticles of smaller sizes and newly formed crystal nuclei decelerate [13]. Eq. 2 shows how the bandgap of nanoparticle E is related to particle radius r:

$$E={E_{bulk}}+\frac{{{\hbar ^2}{\pi ^2}}}{{2e{r^2}}}\left({\frac{1}{{{m_e}{m_o}}}+\frac{1}{{{m_h}{m_o}}}} \right) - \frac{{1.8e}}{{4\pi \varepsilon {\varepsilon _o}r}}$$
2

where {E_{bulk}} is bulk bandgap, \hbar is Planck's constant divided by 2\pi, is elementary electric charge, {m_e} is the electron effective mass, {m_h} is hole effective mass, {m_o} is electron mass, \varepsilon is relative permittivity, and {\varepsilon _o} is the permittivity of vacuum [32–34].

When PVP concentrations were increased except at a 20 mL concentration, absorption spectra showed a redshift suggesting that the particle size of ZnO nanoparticles was decreased.

3.4.1 Direct, Indirect Band Gap and Urbach Energy

An electron band gap, or energy requirement, is the energy required to excite an electron from the highest occupied orbital (HOMO) in the valence band to the lowest unoccupied orbital (LUMO) in the conduction band. Figures 6 and 7 show the {\left({\alpha h\upsilon } \right)^2}and {\left({\alpha h\upsilon } \right)^{\tfrac{1}{2}}} vs. h\upsilon in the direct and indirect band transitions obtained from ZnONPs prepared with different concentrations of PVP. Within the bandgap, there are transitions from the extended valence band to extended conduction band states. The direct and indirect transitions and all other transitions relate to an electromagnetic wave interacting with an electron in the valence band that is excited in the conduction band across the fundamental band gap [35, 36]. As with direct transitions, indirect transitions are accompanied by lattice vibrations simultaneously. Figure 6 shows the weak of {\left({\alpha h\upsilon } \right)^2} at low energy (higher wavelength), representing the transition between one localized state above the valence band and another below the conduction band [35]. Tauc's proposed method uses UV-visible absorption spectra to calculate direct and indirect optical energy gaps for all prepared samples. Eq. 3 can be used to determine the direct optical energy gap [37]

$${\left({\alpha h\upsilon } \right)^{\frac{1}{n}}}=\beta (h\upsilon - {E_g})$$
3

where, {E_g} is the optical band gap, is Plank's constant, \alpha is the absorption coefficient, h\upsilon is the energy incident photon, \beta is a proportionality constant, and represents different values corresponding to allowed electronic transition [36]. When \left({n=1/2} \right)an interband transition is

allowed directly, while \left({n=2} \right) is an indirect interband transition. Additionally, the absorption coefficient \alpha can be calculated by following the following formula

$$\alpha =\frac{{4\pi k}}{\lambda }$$
4

From linear regression of the linear portion of {(\alpha h\upsilon)^2} and {(\alpha h\upsilon)^{1/2}} to zero, the band gap energies were determined using the Tauc plots in Figs. 6 and 7. The point where the line meets the incident photon energy axis represents the direct and indirect band gap energy. Table (2) summarizes the optical band gap calculated by applying the Tauc relationship. Because particle sizes and quantum size effects increased with increasing PVP concentrations, the direct and indirect band gaps decreased except for PVP 20 mL. These results appear to agree with those obtained using TEM and X-rays.

This energy represents the electron transitions from one extended valence band state to another tail state below the conduction band and/or from one extended conduction band state to another tail state above the valence band. During exciting transitions from the top of the valence band to the bottom of the conduction band, low crystalline states and disorders result from localized states caused by defects, measured by an optical parameter known as Urbach energy. This energy results from electron transitions between the extended valence band state to another tail state below the conduction. It can be seen from Fig. 8 that for low photon energies, the Urbach empirical rule describes the dependence of absorption coefficients (α) and photon energies (hv). By using the following relation (5), it can calculate Urbach energy from the absorption spectrum in this regime:

\alpha ={\alpha _o}\exp \left({\frac{{h\upsilon }}{{{E_u}}}} \right)
5

Assume that \alpha is the absorption coefficient, {\alpha _o} is constant, and h\upsilon is the incident photon energy. \ln \alpha versus photon energy h\upsilon plots are used to determine the Urbach energy {E_u}. The reciprocal of the slope obtained by fitting the linear portion of the curve is the Urbach energy {E_u}. Table (2) gives the Urbach energy, which was less than the absorption band edge. Higher {E_u}indicates a low crystallinity and disorder in the nanoparticles

Table 2
Calculation of the absorption peak and direct and indirect band gaps of ZnO nanoparticles prepared at different concentrations of PVP.

Samples	PVP concentrations	Absorption peak (nm)	Direct energy gap (eV)	Indirect energy gap (eV)	Urbach energy
S1	5.00 mL	363.56	4.08	0.91	1.59
S2	10.0 mL	366.64	4.07	0.50	1.79
S3	20.0 mL	362.90	4.10	1.04	3.03
S4	30.0 mL	373.70	3.87	0.23	2.33
S5	40.0 mL	374.90	3.56	0.21	2.34

4. Conclusion

Chemical precipitation methods were used to prepare ZnO nanoparticles capped with PVP. The TEM images were used to confirm distinct shapes, such as spherical, cubic, conical, rod-like, and star-like, as well as to estimate particle size. XRD analysis revealed that ZnONPs form a hexagonal Wuritize structure. According to Scherrer's equation, the particle sizes range from 22 to 27 nm, depending on the PVP content. As shown in FTIR spectra, PVP and ZnONPs have chemically interacted with functional groups. The Quantum Confinement effect was shown to exist by estimating the ultraviolet absorption peaks at a different wavelength. Calculation of the direct and indirect band gaps, as well as Urbach energy, and analysis of the effects of PVP content were discussed.

Declarations

Data Availability

All data are contained within the article.

Authors' contributions

R. Seoudi: Designed and conducted the experiments; analyzed and interpreted the data; wrote the paper.

Lulua Al-Salem: Conducted the experiments; analyzed and interpreted the data; drafted the paper.

Doaa A. Said: Analyzing and interpreting the optical data; reviewing and editing, and reviewing,

Competing interests

The authors declare no competing interests.

References

1. Lulua Al-Salem and Roshdi Seoudi, "Influence of ascorbic acid as a modifier on the particle size and the optical properties of ZnO nanoparticles" Journal of Materials Science: Materials in Electronics, 31(2020)22642–22651
2. Ü. Özgür, Ya. I. Alivov, C. Liu, A. Teke, M. A. Reshchikov, S. Doğan, V. Avrutin, S.-J. Cho, and H. Morkoç, "A comprehensive review of ZnO materials and devices. J. Appl. Phys. 98 (2005) 041301.
3. S. Muthukumar, Haifeng Sheng, Jian Zhong, Zheng Zhang, N.W. Emanetoglu, and Yicheng Lu, "Selective MOCVD growth of ZnO nanotip", IEEE Trans Nanotechnol. 2 (2003)50–58.
4. Gurushankar K, Jeyavijayan S, Gohulkumar M, and Viswanathan K, "Synthesis, Optical and Morphological Studies of ZnO Nanoparticles Capped with PVP as a Surfactant", Int J Chem Sci. 16(2018) 240

5. J Theerthagiri, Sunitha Salla, R A Senthil, P Nithyadharseni, A Madankumar, Prabhakarn Arunachalam, T Maiyalagan, Hyun-Seok Kim, "A review on ZnO nanostructured materials: energy, environmental and biological applications", Nanotechnology, 30(2019)392001.
6. M.S. Ren, J.M. Song, Y.L. Shi, Y.B. Xiang, G. Hu, "Synthesis of zinc pyrovanadate3D flower-like microspheres and their photocatalytic properties", J. Cryst. Growth, 402 (2014) 119–123.
7. Y Zhang, S Li, G Goh, and S Tripathy, "Hydrothermal epitaxy of ZnO:Co diluted magnetic semiconducting single crystalline films", Appl. Phys. Lett, 93 (2008)10251.
8. C Knies, M T Elm, P J Klar, J Stehr, D M Hofmannn and N Romanov 2009 J.Appl. Phys. 105 073918–7.
9. P. Bindu, and S. Thomas, "Optical Properties of ZnO Nanoparticles Synthesised from a Polysaccharide and ZnCl2" ACTA PHYSICA POLONICA A 131(2017) 1474–1478
10. Wang C, Guan L, Mao Y, et al. Optical nonlinearity of ZnS–polyvinyl pyrrolidone nanocomposite suspension. J. Phys D: Appl Phys. 2009;42:45403.
11. Wang CE, Shen E, Gao WL. Controllable synthesis of ZnO nanocrystals via a surfactant-assisted alcohol thermal process at a low temperature. Mater Lett. 2005;59:2867–71.
12. Ajji Z. Grafting of poly (vinyl pyrrolidone) with citric acid using gamma irradiation. Nucl Instrum. Methods Phys Res B. 2007;265:179–82.
13. Yuliah Y, Bahtiar A. Synthesis and characterization of PVP-capped ZnO particles and its blend with poly (3-hexylthiophene) for hybrid solar cells application. Padjadjaran Int Phys Symp. (PIPS-2013) AIP Conf Proc. 2013;1554:139 – 42.
14. Cao G. Nanostructures and nanomaterials: Synthesis, properties and applications. Imper Coll Press. London. 2006.
15. Janotti, A.; van de Walle, C.G. Oxygen vacancies in ZnO. Appl. Phys. Lett. 2005, 87, 122102.
16. Meulenkamp, E.A. Synthesis and growth of ZnO nanoparticles. J. Phys. Chem. B 1998, 102, 5566–5572.
17. Kavitha, M.K.; Jinesh, K.B.; Philip, R.; Gopinath, P.; John, H. Defect engineering in ZnO nanocones for visible photoconductivity and nonlinear absorption. Phys. Chem. Chem. Phys. 2014, 16, 25093–25100.
18. Singh, A.K.; Viswanath, V.; Janu, V.C. Synthesis, effect of capping agents, structural, optical and photoluminescence properties of ZnO nanoparticles. J. Lumin. 2009, 129, 874–878.
19. Tachikara, S.; Noguchi, A.; Tsuge, T.; Hara, M.; Odawara, O.; Wada, H. Optical properties of ZnO nanoparticles capped with polymers. Materials 2011, 4, 1132–1143.
20. Xiong, H.-M. Photoluminescent ZnO nanoparticles modified by polymers. J. Mater. Chem. 2010, 20, 4251–4262.
21. Gutul, T.; Rusu, E.; Condur, N.; Ursaki, V.; Goncearenco, E.; Vlazan, P. Preparation of poly (n-vinylpyrrolidone)-stabilized ZnO colloid nanoparticles. Beilstein J. Nanotechnol. 2014, 5, 402–406.

22. Kamari, H.; Al-Hada, N.; Saion, E.; Shaari, A.; Talib, Z.; Flaifel, M.; Ahmed, A. Calcined solution-based PVP influence on ZnO semiconductor nanoparticle properties. Crystals 2017, 7, 2.
23. OkSik Kim, JinBeom Kwon, SaeWan Kim, Binrui Xu, KyeongHo Seo, CheolEon Park, WooJong Do, JinHyuk Bae and ShinWon Kang, "Effect of PVP-Capped ZnO Nanoparticles with Enhanced Charge Transport on the Performance of P3HT/PCBM Polymer Solar Cells", Polymers 2019, 11, 1818; doi:10.3390/polym11111818
24. Joint committee on powder Diffraction Standards,Powder Diffraction File no 36–1451.
25. M. Sudha,S. Senthilkumar, R. Hariharan, A. Suganthi and M. Rajarajan, "Controlled reduction of the deleterious effects of photocatalytic activity of ZnO nanoparticles by PVA capping", Sol-Gel sci Technol, 61(2011)14–22.
26. Ahmad Monshi, Mohammad Reza Foroughi and Mohammad Reza Monshi, "Modified Scherrer Equation to Estimate More Accurately Nano-Crystallite Size Using XRD ", World Journal of Nano Science and Engineering, 2 (2012)154–160.
27. Salih Salih, Mizi Fan, Dasong Dai and Biao Huang, "Fourier Transform Infrared Spectroscopy for Natural Fibers", Fourier Transform Materials Analysis, DOI: 10.5772/35482, (2012) 46–68.
28. Pesika, N.S.; Stebe, K.J.; Searson, P.C. Determination of the particle size distribution of quantum nanocrystals from absorbance spectra. Adv. Mater. 2003, 15, 1289- Interpreted
29. Sze-Mun Lam, Ming-Wei Kee, Jin-Chung Sin,"Influence of PVP surfactant on the morphology and properties of ZnO micro/nanoflowers for dye mixtures and textile wastewater degradation",Materials Chemistry and Physics, 212 (2018) 35–43.
30. Z.J. Yu, M.RajeshKumar, D.L.Sun, L.T.Wang, R.Y.Hong, "Large scale production of hexagonal ZnO nanoparticles using PVP as a surfactant", Materials Letters, 166 (2016) 284–287.
31. Thilagavathi Thirugnanam," Effect of Polymers (PEG and PVP) on Sol-Gel Synthesis of Microsized Zinc Oxide", Journal of Nanomaterials, 362175 (2013)1–7.
32. Pesika, N.S.; Stebe, K.J.; Searson, P.C. Determination of the particle size distribution of quantum nanocrystals from absorbance spectra. Adv. Mater. 2003, 15, 1289–1291.
33. Hu, Z.; Oskam, G.; Searson, P.C. Influence of solvent on the growth of ZnO nanoparticles. J. Collo. Inter. Sci. 2003, 263, 454–460.
34. Brus, L.E. Electronic wave-functions in semiconductor clusters—Experiment and theory. J. Phys. Chem. 1986, 90, 2555–2560.
35. Singh, J., (Eds.), Optical Properties of Condensed Matter and Applications, Wiley: 2006
36. Adachi, S., (Eds.), Optical Properties of Crystalline and Amorphous Semiconductors: Materials and Fundamental Principles, Springer, New York, 1999.
37. Tauc, J.; Grigorovici, R.; Vancu, A. Optical Properties And Electronic Structure of Amorphous Germanium. Phys. Status Solidi B 1966, 15, 627–637.

Figures

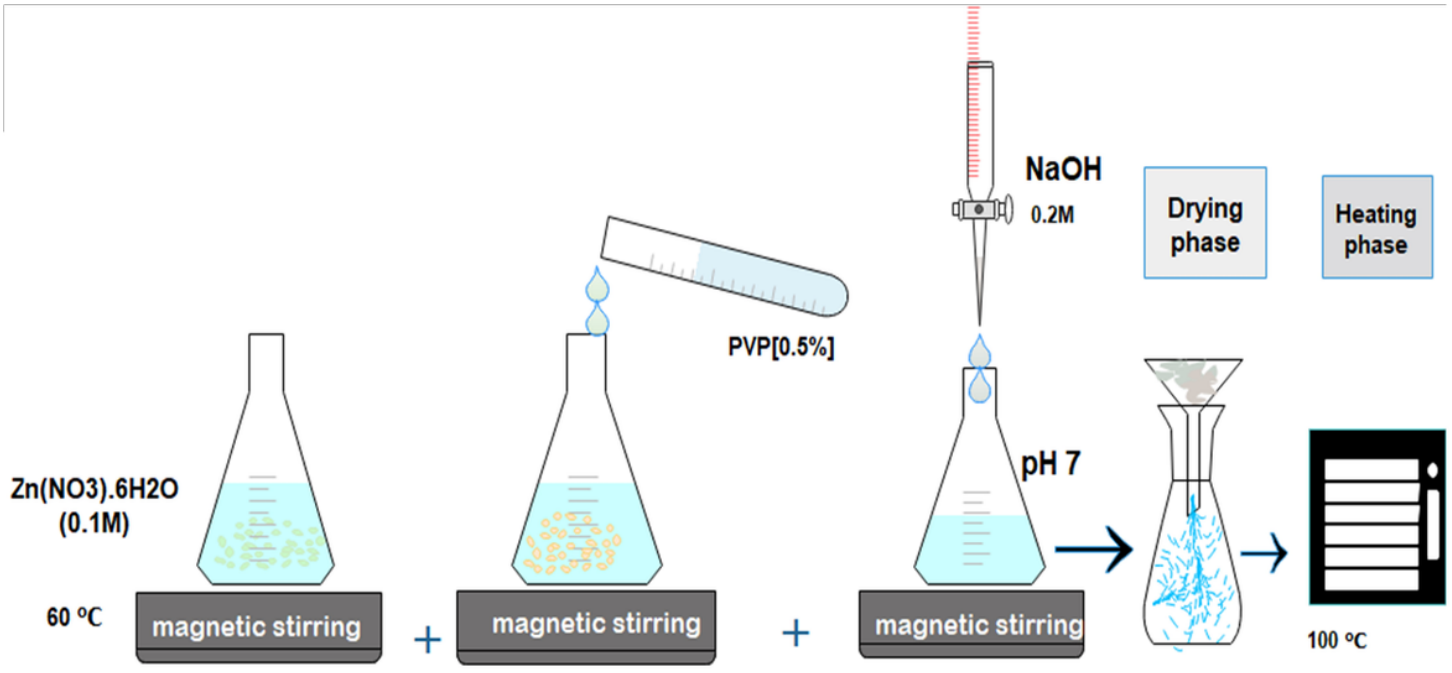

Figure 1

Figure 1

shows the steps for preparing ZnO nanoparticles.

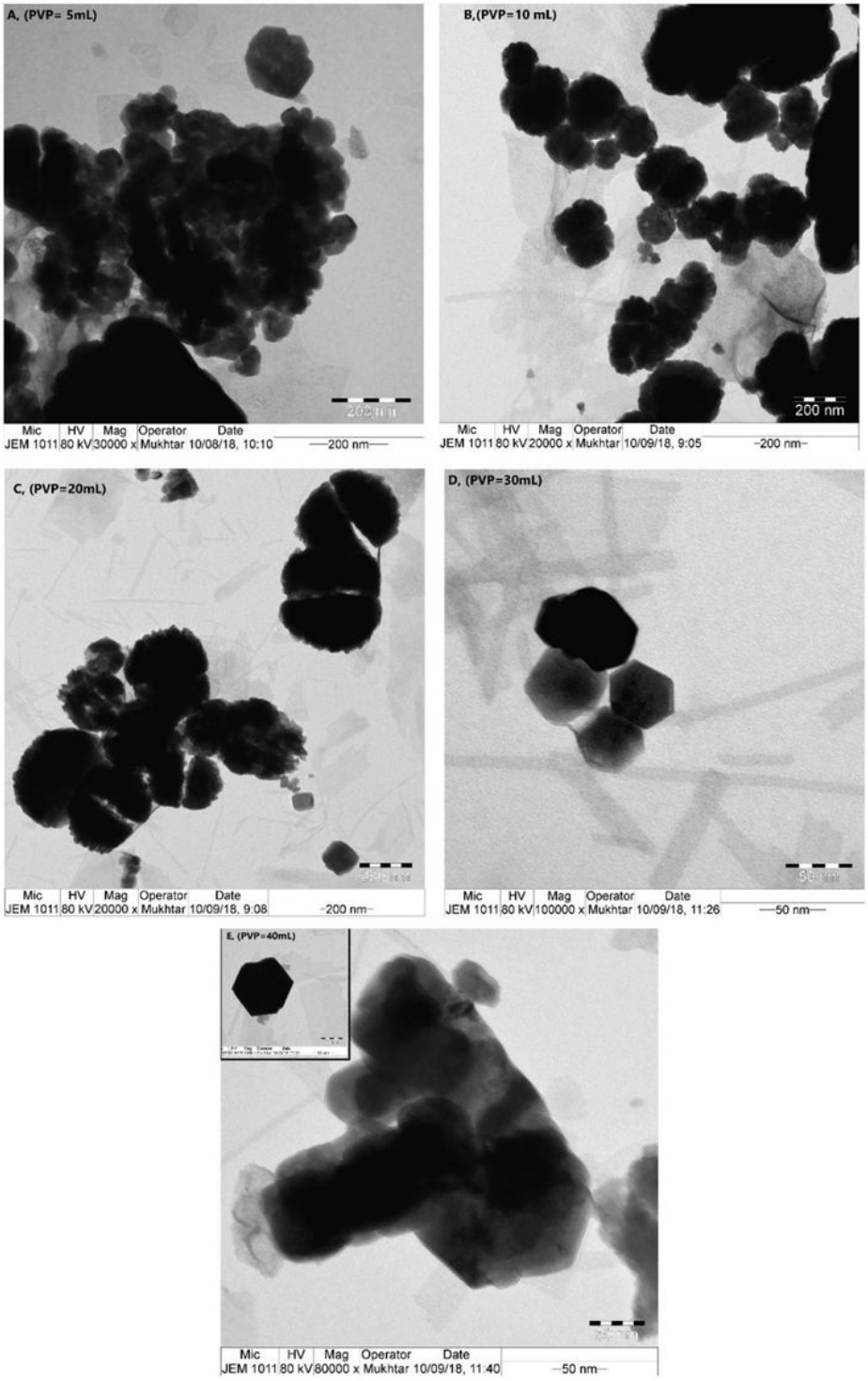

Figure (2:a-e)

Figure 2

(A-E): TEM images (A-E) of zinc oxide nanoparticles prepared at different concentrations of the polymer (PVP).

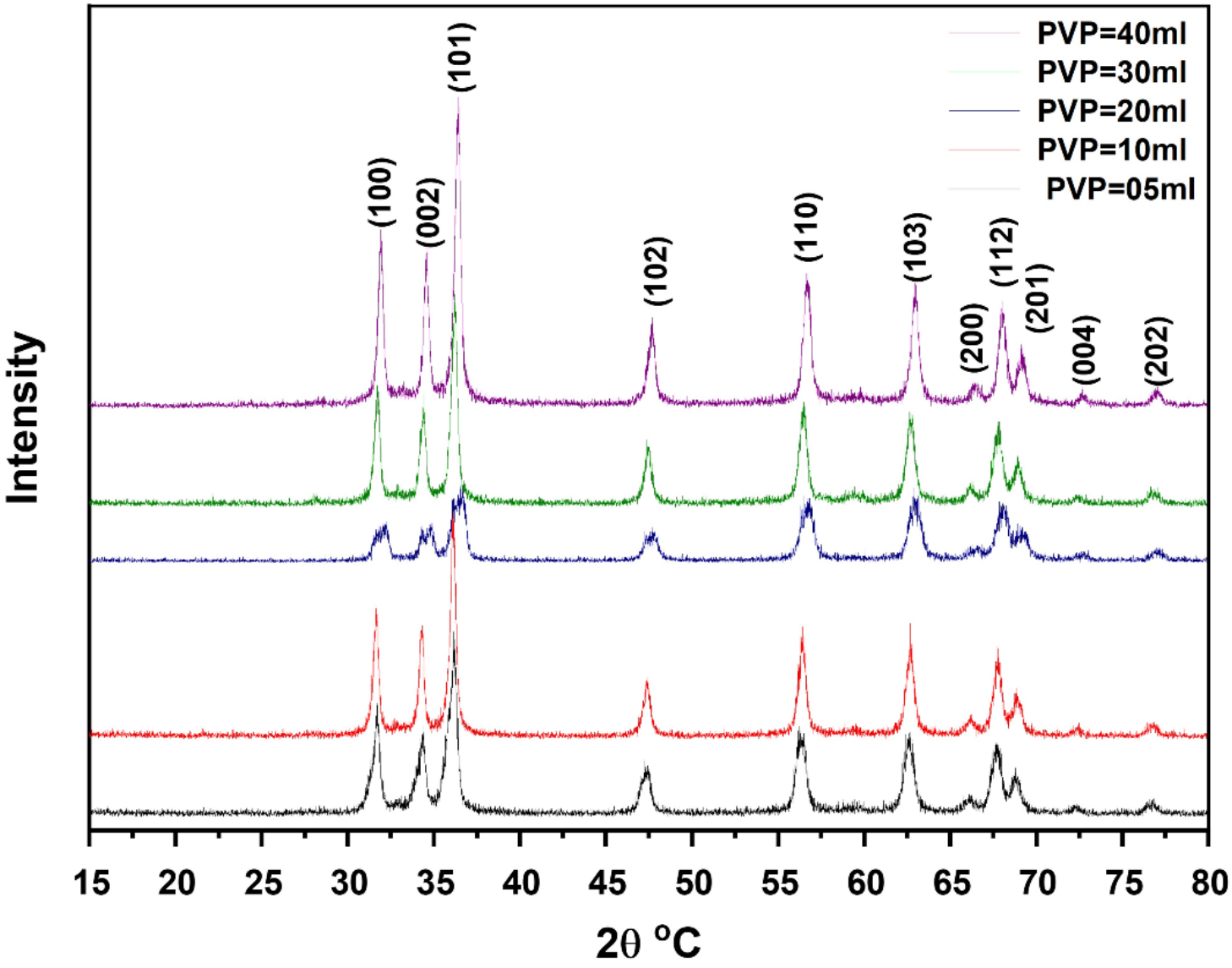

Figure 3

Figure 3

X-ray diffraction pattern of ZnONPs prepared at different PVP concentrations.

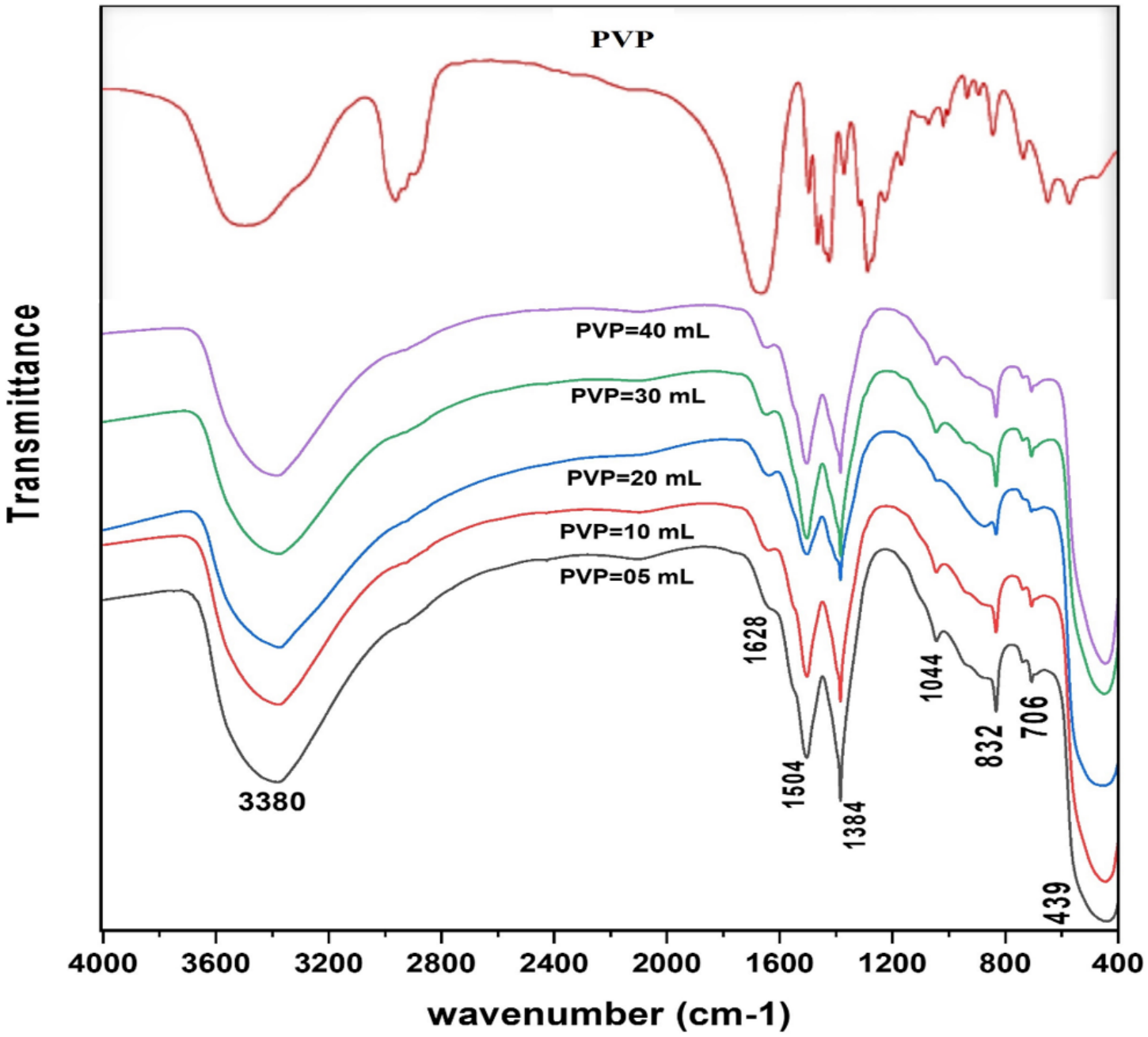

Figure 4

Figure 4

Infrared spectra of ZnO nanoparticles prepared with various concentrations of PVP.

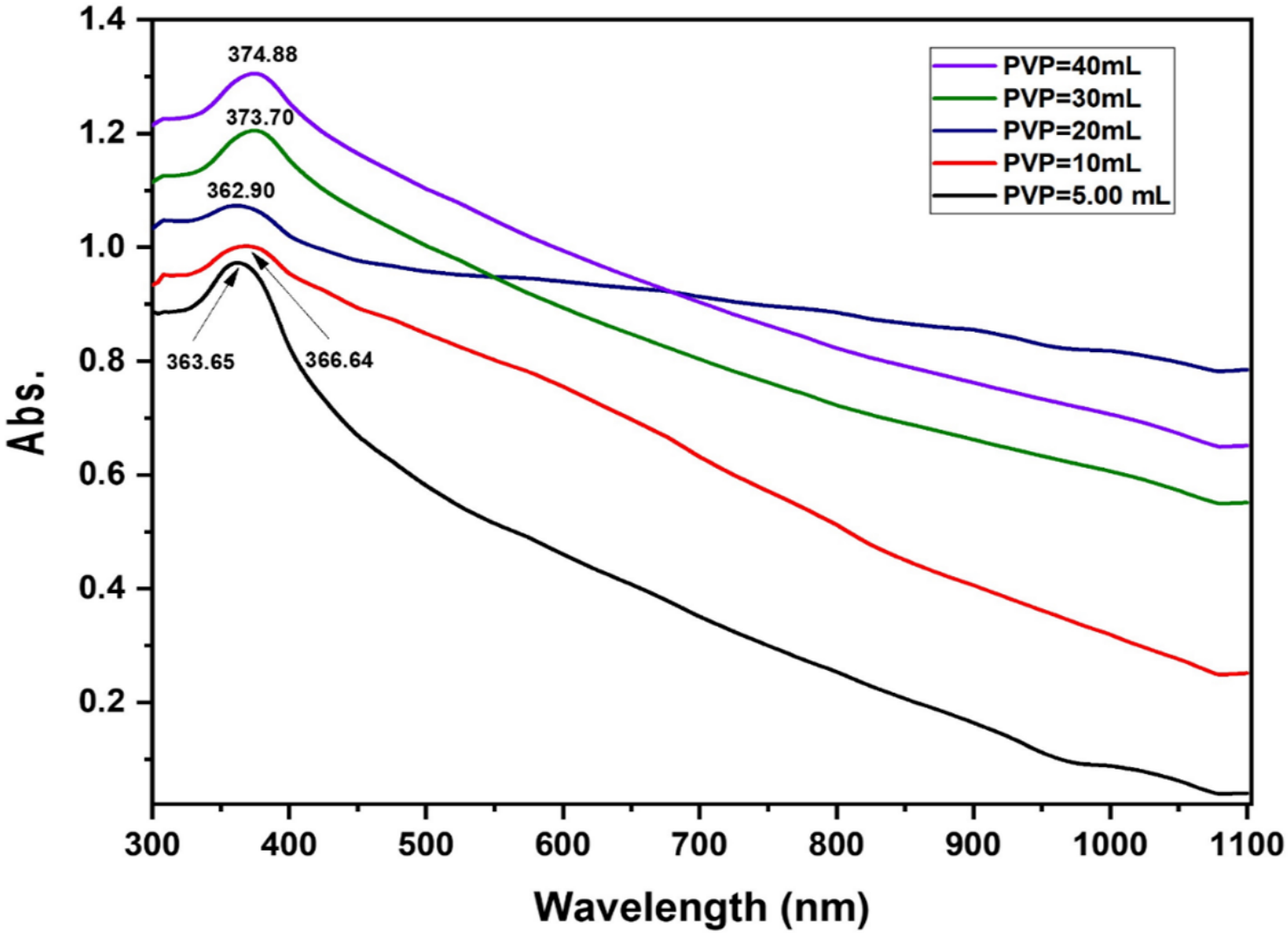

Figure 5

Figure 5

Absorption spectra of ZnO nanoparticles prepared at different

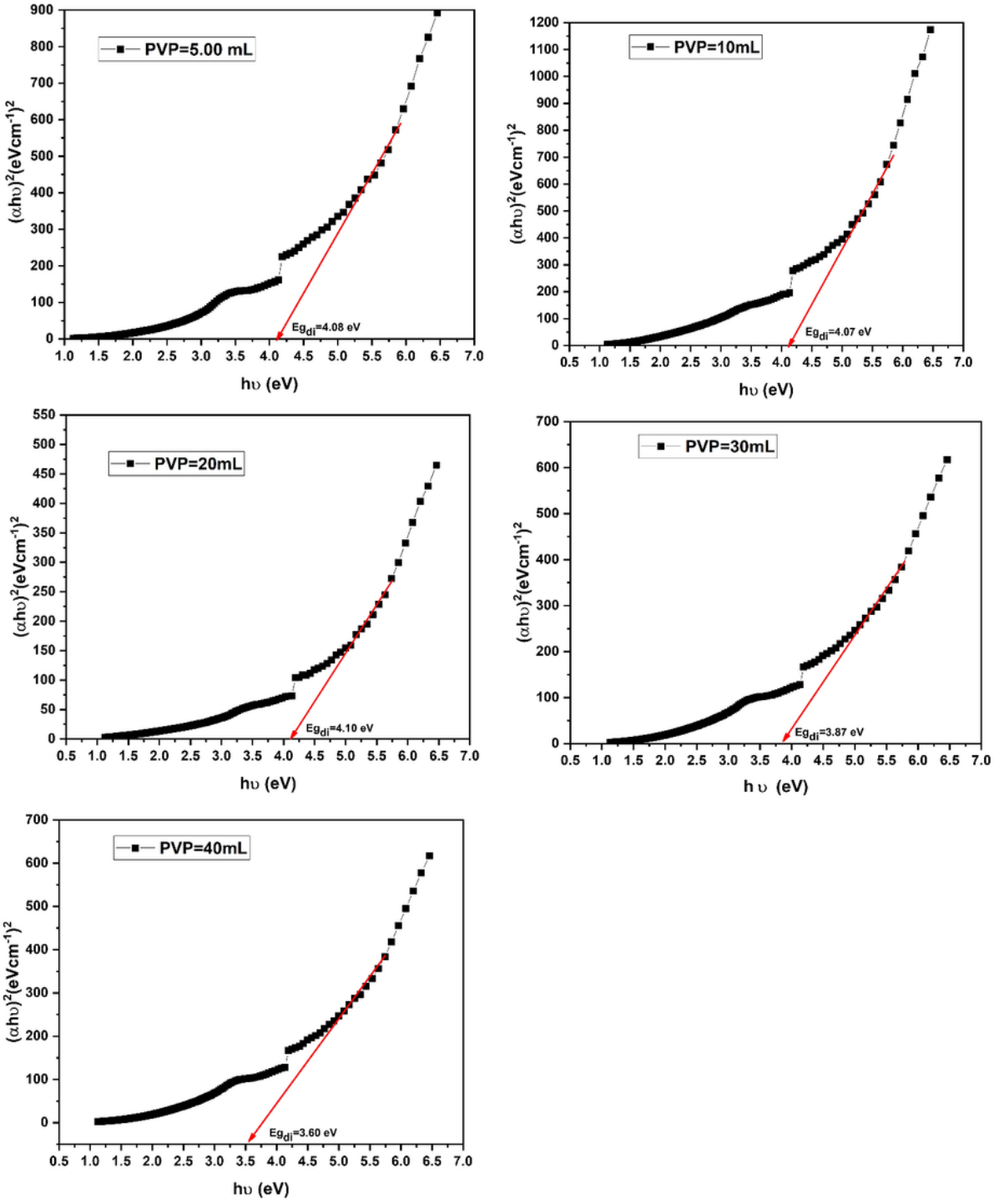

Figure (6)

Figure 6

Direct band gap energy of ZnONPs prepared at various PVP concentrations

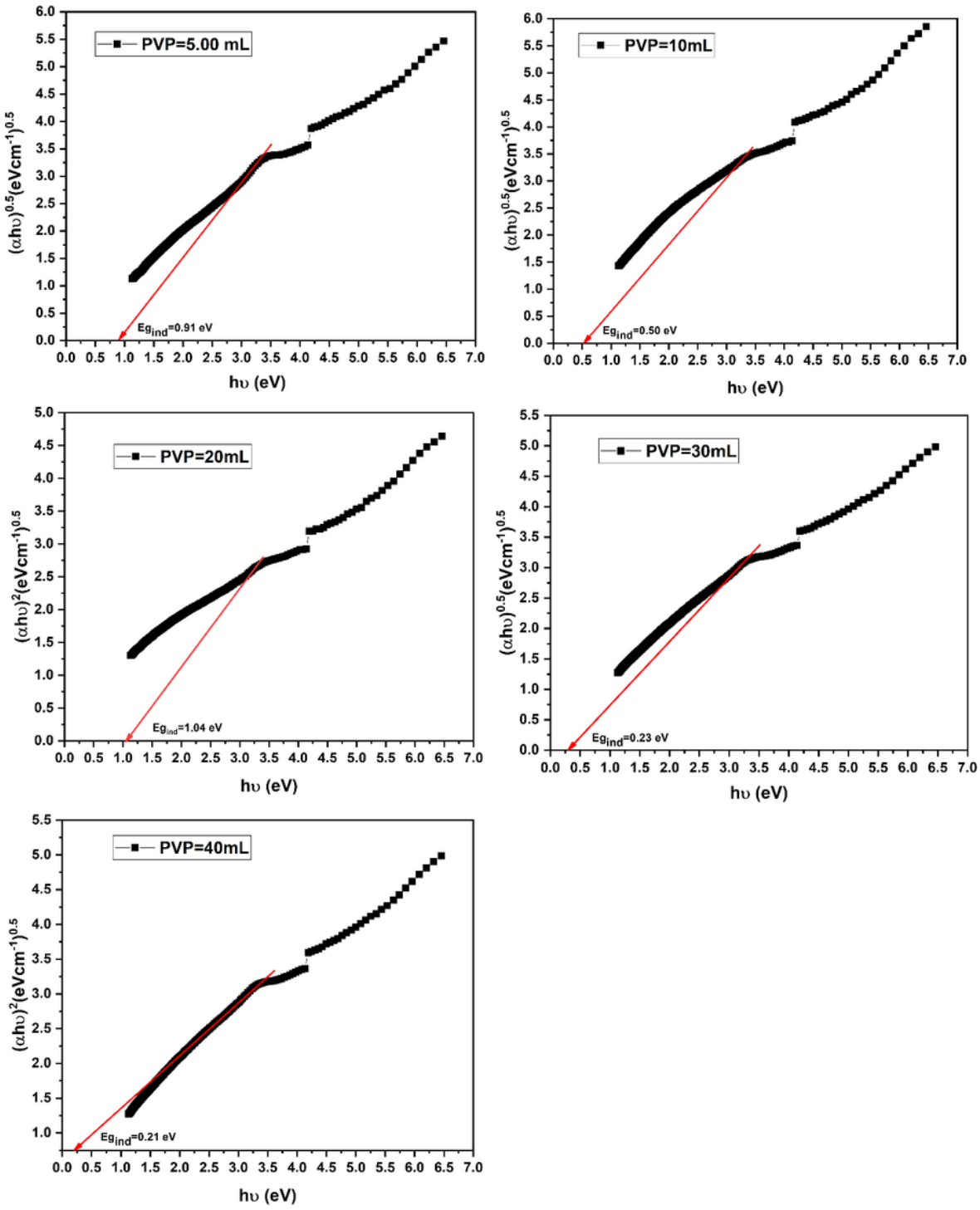

Figure (7)

Figure 7

Indirect band gap energy of ZnONPs prepared at different PVP concentrations.

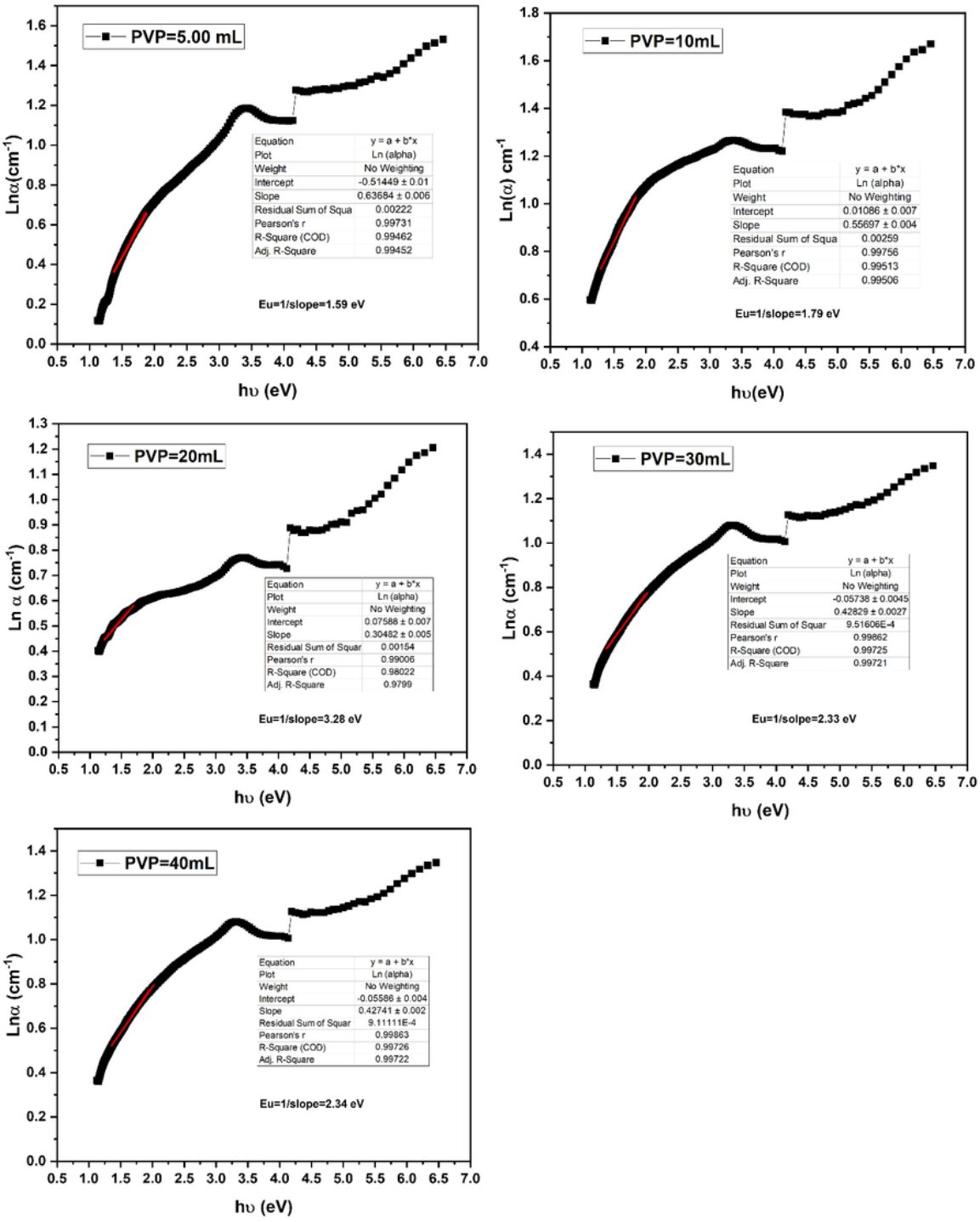

Figure (8)

Figure 8

Urbach energies for ZnONPs prepared at different PVP concentrations